Observing angular precession of a Rydberg wave packet due to spin-orbit coupling by orthogonally polarized weak half-cycle pulses

H. Wen, S. N. Pisharody, J. M. Murray, and P. H. Bucksbaum
FOCUS Center, Department of Physics, University of Michigan, Ann Arbor, Michigan 48109-1120, USA
(Received 16 March 2006; published 15 May 2006)

We investigate the response of an *np* Rydberg wave packet to orthogonally polarized weak half-cycle pulses (HCPs) over the course of its field-free evolution. The population redistribution from *p* to *s* states is highly sensitive to the polarization of the HCP and changes with the precession of the electron orbits due to the spin-orbit coupling. We obtain the selection rules and give an intuitive classical interpretation of angular momentum redistribution by a HCP.

DOI: 10.1103/PhysRevA.73.052504 PACS number(s): 32.10.Fn, 32.80.Qk, 32.80.Lg, 32.80.Rm

I. INTRODUCTION

Coherent control and manipulation of atomic and molecular systems have been of growing interest with recent advances in technology. Novel electromagnetic fields such as half-cycle pulses (HCPs) have been employed to generate target quantum systems and probe their dynamics, e.g., Refs. [1–5]. A HCP is able to interact with a bound electron throughout its orbit, unlike ultrafast multicycle laser pulses which only probe the electron near the nucleus [6]. If the interaction time is much shorter than the interested dynamics of the system, a HCP can be modeled as an impulsive momentum transfer. The impulse has been used to retrieve the momentum distribution of electron wave packets [7]. Multiple HCPs with different polarizations can be used to recover the momentum distribution in multiple dimensions [8,9]. If the strength of a HCP is far below that required to directly ionize the atoms, the HCP coherently redistributes the population to neighboring *n* states as well as different angular momentum manifolds [10,11]. In this work, HCPs with different polarizations irradiate an *np* Rydberg wave packet precessing due to spin-orbit (SO) coupling. The angular momentum redistribution by the HCP is highly polarization sensitive. The selection rules for HCP-induced state redistribution are obtained using a quantum mechanical approach and an intuitive classical interpretation is given for our observations.

The spin of the electron is not usually considered in the analysis of Rydberg wave packet motion because of its negligible effect on the dynamics. Radial [12] and angular localization [13] and collapses and revivals [14,15] have been well understood without considering SO coupling. SO coupling can be enhanced and gives rise to observable effects in high atomic number(Z) atoms [16,17]. The angular precession of a Rydberg wave packet can be detected in the redistribution of population following a HCP interaction. This is sensitive to HCP polarization and yields information on the shape of the wave packet that cannot be obtained using traditional two-pulse wave packet interference [18–20]. The HCP method also circumvents the need for high time delay resolution and the long acquisition times that are required in interferometric two-pulse experiments.

This paper is organized as follows. In Sec. II, the spin-orbit effect on a Rydberg wave packet is discussed; in Sec. III, we describe the experiment and the results; and in Sec. IV, the selection rules of state redistribution by HCPs are derived to understand the data. The discussions and conclusions are given in Sec. V.

II. ANGULAR PRECESSION OF A RADIAL WAVE PACKET

SO coupling causes the electron spin to influence the orbital degrees of freedom. A radial wave packet excited by an ultrafast pulse can be reshaped substantially due to SO coupling. We can understand when and how SO coupling affects the dynamics of Rydberg wave packets using a similar approach to that in Refs. [19,20].

Let us first consider a hydrogen atom, ignoring the electron spin. The Hamiltonian of the electron is simply $H=\frac{p^2}{2}-\frac{1}{r}$ (atomic units are used throughout) and the eigenstates are $\Psi_{n,\ell,m}$, where n, ℓ, m are the radial, angular, and magnetic quantum numbers, respectively. A wave packet is usually prepared by exposing atoms or molecules to a laser pulse whose bandwidth covers several energy eigenstates. For example, a radial wave packet excited by a short pulse polarized along quantization axis ($\hat{z}$) with a one photon transition from the *s* state is a coherent superposition of several *np* states, $\Sigma_n \Psi_{n,\ell=1,m=0}$.

If the electron spin is included, the effective Hamiltonian of the electron is modified due to the intrinsic magnetic field generated by the electron motion. The corresponding eigenstates are ψ_{n,j,m_j}, where $j=\ell+s,\ldots,|\ell-s|$ and $m_j=j,\ldots,-j$. For simplicity, we examine one of the n-state $\Psi_{n,\ell=1,m=0}$ in the wave packet and omit n throughout. The results can be easily generalized for a radial wave packet composed of several n states. The intensity of the excitation laser is usually in the nonrelativistic region and thus only affects the spacial wave functions but not the spin. In the uncoupled basis (denoted as Ψ_{ℓ,m,m_s}), the spin-up state at time zero can be written as $\Phi(t=0)=\Psi_{1,0,\uparrow}$. In order to see how the energy eigenstates are populated, we rewrite the wave function in the coupled basis (denoted as ψ_{j,m_j}),

$$\Phi(t=0)=\sqrt{\frac{2}{3}}\psi_{\frac{3}{2},\frac{1}{2}}-\sqrt{\frac{1}{3}}\psi_{\frac{1}{2},\frac{1}{2}}. \quad (1)$$

Equation (1) shows that the excitation ratio of $P_{3/2}$ to $P_{1/2}$ is 2:1. After the excitation, the wave function starts to evolve

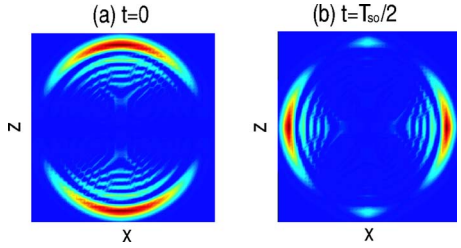

FIG. 1. (Color online) The density plot of $28p$ wave function in $x-z$ plane: (a) at $t=0$ and (b) at $t=T_{SO}/2$.

by acquiring dynamical phases on the eigenstates

$$\Phi(t) = \sqrt{\tfrac{2}{3}}e^{-i\omega_2 t}\psi_{\frac{3}{2},\frac{1}{2}} - \sqrt{\tfrac{1}{3}}e^{-i\omega_1 t}\psi_{\frac{1}{2},\frac{1}{2}}, \tag{2}$$

where ω_1 and ω_2 are the energies associated with $P_{1/2}$ and $P_{3/2}$. To see how the wave packet evolves, we need to separate the spin from the spacial wave function and work in the uncoupled basis

$$\Phi(t) = \frac{\sqrt{2}}{3}(e^{-i\omega_2 t} - e^{-i\omega_1 t})\Psi_{1,1,\downarrow} + \left(\frac{2}{3}e^{-i\omega_2 t} + \frac{1}{3}e^{-i\omega_1 t}\right)\Psi_{1,0,\uparrow}. \tag{3}$$

For the spin-down state, we can obtain similar results by replacing $\Psi_{1,0,\uparrow}, \Psi_{1,1,\downarrow}$ with $\Psi_{1,0,\downarrow}, \Psi_{1,-1,\uparrow}$ in Eq. (3). After grouping the same $|m|$ states, the population of $m=0$ and $|m|=1$ states of the wave packet can be calculated as

$$P_{\ell=1,m=0}(t) = \tfrac{5}{9} + \tfrac{4}{9}\cos[(\Delta\omega t)], \tag{4}$$

$$P_{\ell=1,|m|=1}(t) = \tfrac{4}{9}[1 - \cos(\Delta\omega t)], \tag{5}$$

where $\Delta\omega = \omega_1 - \omega_2$.

Evidently, 89% of the population oscillates between $m=0$ and $|m|=1$ states. This implies the electron clouds align parallel and perpendicular to the atomic axis alternatively (Fig. 1). If more than one n state is involved, as in a radial wave packet, both radial breathing and angular precession are expected. Such a wave packet provides an ideal testing ground to investigate the polarization dependence of the angular momentum state redistribution due to HCPs. The time dependent signal can be obtained for the fixed polarization of HCPs thanks to the oscillation of the orientation of the electron clouds.

The precession time T_{SO} is simply $2\pi/\Delta E_{SO}$, where ΔE_{SO} is the energy splitting due to SO coupling. In hydrogen atoms, the precession time is $\sim n^3\alpha^{-2}Z^{-4}$, where α is the fine structure constant. Since it is several orders of magnitude longer than the interested dynamics (e.g., classical Kepler period T_{cl}), the SO effect can be safely ignored. In alkali atoms, however, the precession time is shortened dramatically due to quantum defects. For example, T_{SO} associated with p splitting in cesium atoms is determined by

$$\Delta E_{SO} = \frac{1}{2(n-\delta_2)^2} - \frac{1}{2(n-\delta_1)^2}, \tag{6}$$

where δ_1 and δ_2 are the first order quantum defects of $P_{1/2}$ and $P_{3/2}$. For $n\to\infty$, T_{SO} is $\sim$570 times shorter than that of hydrogen atoms while T_{cl} remains the same. Practically, we obtain $T_{SO}\approx 30T_{cl}$ for $28p$ state in cesium atoms. Therefore, SO effects need to be considered in alkali-metal atoms when T_{SO} is comparable in duration to the interesting dynamics such as Kepler motion and wave packet collapses and revivals.

III. EXPERIMENT AND RESULTS

We use cesium atoms from an effusive source to generate Rydberg wave packets in a two-step process. First, the $7s$ launch state is populated using a two-photon transition from $6s$ ground state by a tightly focused pulse centered around 1079 nm. Next, a spectrally shaped 800 nm pulse is polarized along the quantization axis ($\hat{z}$) and populates the energy eigenstates in the range of $n=27,\ldots,32$. The relative polarizations of the laser pulses ensures that only the $m=0$ component is directly excited in the Rydberg wave packet. A HCP with a full width at half maximum (FWHM) of $\sim$400 fs is generated by illuminating on a high-voltage biased GaAs wafer with a 50 fs, 800 nm pulse. The wafer is oriented either parallel or perpendicular to the quantization axis and the HCPs collinear with the laser beam interact with atoms at various delays. The peak field of the HCP is about 1 kV/cm and corresponds to an impulse of 0.002 a.u. As a result of SO coupling, the relative angle between electron orbits and the HCP changes over the course of the wave packet evolution. The ionization field along $\hat{z}$ axis is applied ~ 8 μs later to record the individual state populations. The state-selective field-ionization spectra as a function of the HCP delay are plotted as "quantum carpets" [5] in Figs. 2(a) and 2(b). The p and s state populations are clearly resolved. The line-out of the s state population as a function of the HCP delay is plotted in Figs. 2(c) and 2(d). The 2.4 ps fast oscillation corresponds to the Kepler motion while the 68 ps envelope modulation matches the energy splitting of $28P_{3/2}$ and $28P_{1/2}$ states. Around the time of excitation of the wave packet, the contrast of fast oscillation reaches its maximum if a $\hat{z}$-polarized HCP is applied while it is around zero if an $\hat{x}$-polarized HCP is applied. At the time delay corresponding to one half of the envelope modulation period, the reverse situation occurs. Recalling that the wave packet only has an $m=0$ component at time-zero and 89% $|m|=1$ component at half of the precession time, we find that a HCP redistributes population from p to s states when it is aligned along the electron clouds. We can understand this using both quantum mechanical and classical approaches described in the next section.

IV. SELECTION RULES OF HCP-INDUCED STATE REDISTRIBUTION

The strong polarization dependence of the redistribution from p to s can be understood using an impulsive model of a HCP. A HCP acts as an operator $e^{-i\vec{Q}\cdot\vec{r}}$ on the wave function, where $\vec{Q} = -\int\vec{F}(t)dt$, $\vec{F}(t)$ is the time-dependent electric field and $\vec{r}$ is the position operator of the electron. The transition strength due to the HCP is obtained by evaluating matrix

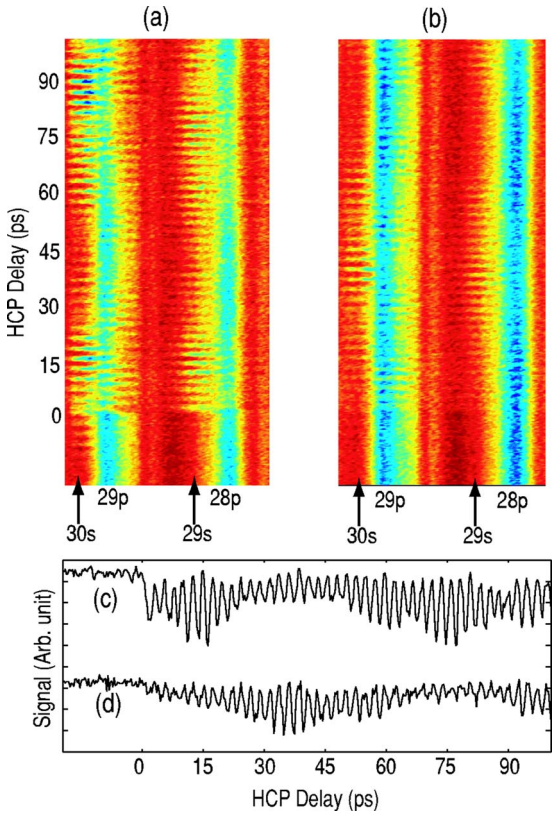

FIG. 2. (Color online) The HCP-induced state-resolved ionization signal as the function of the HCP delay. (a) A $\hat{z}$-polarized HCP is applied; (b) An $\hat{x}$-polarized HCP is applied; (c) the line-out of 29s state in (a); and (d) the line-out of 29s state in (b).

elements $\langle n',\ell',m'|e^{-i\vec{Q}\cdot\vec{r}}|n,\ell,m\rangle$. The uncoupled basis is utilized since the HCP operates on the spatial wave function. For a $\hat{z}$-polarized HCP, the Taylor expansion of e^{-iQz} indicates the matrix elements only survive if $\ell=\ell'\pm 0,1,2\ldots$ and $m=m'$. For an $\hat{x}$-polarized HCP, we need to inspect the matrix elements further to obtain the selection rules. Using $3j$ symbols and the expansion

$$e^{i\vec{Q}\cdot\vec{r}}=4\pi\sum_{L=0}^{\infty} i^L j_L(Qr)\sum_{M=-L}^{L} Y^*_{L,M}(\theta',\phi')Y_{L,M}(\theta,\phi),$$

where $\theta'=\pi/2,\phi'=0$ for an $\hat{x}$-polarized HCP and θ,ϕ are related to the electron position $\vec{r}$, the integral $\langle n',l',m'|e^{-iQx}|n,l,m\rangle$ can be written as

$$\begin{aligned}\langle n',l',m'|e^{-iQx}|n,l,m\rangle &= (-1)^{m'}4\pi\sum_{L=0}^{\infty} i^L R_{n\ell,n'\ell',L}\sum_{M=-L}^{L} Y^*_{L,M}\left(\frac{\pi}{2},0\right)\\ &\times\sqrt{\frac{(2\ell'+1)(2\ell+1)(2L+1)}{4\pi}}\\ &\times\begin{pmatrix}\ell' & \ell & L\\ 0 & 0 & 0\end{pmatrix}\begin{pmatrix}\ell' & \ell & L\\ -m' & m & M\end{pmatrix},\end{aligned}\quad(7)$$

where $R_{n\ell,n'\ell',L}$ denotes the nonzero radial integral. The two

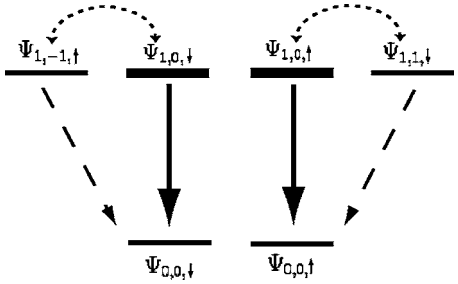

FIG. 3. The diagram to illustrate the detection scheme of $m=0$ and $|m|=1$ components of wave packets. The bold lines indicate the population in $m=0$ states at the moment of excitation. The solid arrows indicate the coupling due to $\hat{z}$-polarized HCP. The dashed arrows indicate the coupling due to an $\hat{x}$-polarized HCP. The dotted arrows indicate the population oscillation between $m=0$ and $|m|=1$ states due to the spin-orbit coupling.

$3j$ symbols are nonzero if and only if $L+\ell+\ell'$ is even and $m'-m=M$. Combining them with the fact $Y^*_{L,M}(\pi/2,0)$ is nonzero if only if $L+M$ is even, we know that the integral [Eq. (7)] is nonzero if and only if $\Delta(\ell+m)$ is even. The same selection rules hold for a $\hat{y}$-polarized HCP because of the azimuthal symmetry of the electron clouds. The selection rules of HCP redistribution can be summarized

$$\Delta\ell=0,1,2\ldots \text{ and } \Delta m=0,\quad \hat{z}-\text{polarized HCP},\quad(8)$$

$$\Delta(\ell+m)=0,2,4\ldots,\quad \hat{x}(\hat{y})-\text{polarized HCP}.\quad(9)$$

Therefore, a $\hat{z}$-polarized HCP applied to a Rydberg np wave packet is only able to populate s states from $m=0$ states (Fig. 3, solid arrows). Monitoring the population of s states while delaying the HCP, the variation of $m=0$ state population can be recorded at any instant. On the other hand, if an $\hat{x}$-polarized HCP is applied, s states couple to $|m|=1$ states instead (Fig. 3, dashed arrows). Thus, the changing population of s states reflects the population variation of $|m|=1$ states. The SO-interaction-induced coupling between $m=0$ and $|m|=1$ states is indicated by the dotted double arrows in Fig. 3. We can detect $m=0$ and $|m|=1$ states population selectively by rotating the polarization of HCPs. The π phase shift in the population oscillation of $m=0$ and $|m|=1$ states is evident for orthogonally polarized HCPs.

The HCP strength ($Q=0.002$ a.u.) is chosen to be large enough to couple strongly the nearest-neighbor np states to s states to reveal the Kepler motion of the electron [5], but small enough not to mix the more distant np states that would cause the rapid collapse of the spin-orbit wave packet. Thus, both radial and angular motion can be recorded in a single scan (Fig. 2).

In the classical picture, the electron can be modelled as a charged particle moving around the nucleus. The p orbit is an ellipse which is parallel to the $\hat{z}$ axis if $m=0$ but perpendicular to the $\hat{z}$ axis if $|m|=1$. A kick parallel to the p orbit is able to accelerate or slow the electron and thus alter its orbit to higher angular momentum orbit d or to lower angular momentum orbit s, depending on the direction of the electron velocity at the moment of the kick. Therefore, $p\rightarrow s$ transitions are allowed. However, the electron is only accelerated

to higher angular momentum orbits by a perpendicular kick because of its small momentum along the kicked direction. In this case, no redistribution to lower angular momentum orbit(s) is allowed.

It is instructive to apply the first order selection rules to the momentum distribution due to HCPs. The momentum distribution around zero is peaked if $\ell+m$ is even but zero if $\ell+m$ is odd [21]. Therefore, a $\hat{z}$-HCP dominantly redistributes the population to the opposite parity of $\ell+m$ and thus changes the momentum distribution, but an $\hat{x}$-HCP keeps the parity of $\ell+m$ and makes almost no change to the momentum distribution along z direction [22].

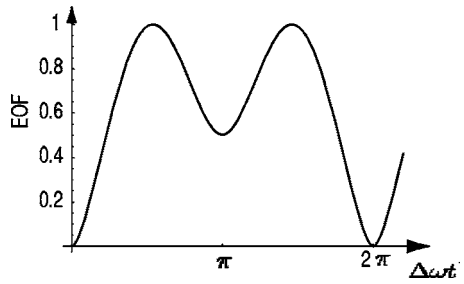

FIG. 4. The entanglement of formation (EOF) of Eq. (3) as a function of $\Delta\omega t$.

V. DISCUSSIONS AND CONCLUSIONS

The interaction between the spin and the orbital motion leads to spin-orbit entanglement. The degree of entanglement changes with time. At time zero, there is only an $m=0$ component and the spin is not entangled with the spatial motion of the electron. At $t=\cos^{-1}(-\frac{1}{8})/\Delta\omega$, taking the state [Eq. (3)] for example, it reaches the maximally entangled state $\Phi(t)=\frac{1}{\sqrt{2}}(|m=0,\uparrow\rangle+e^{i\delta}|m=1,\downarrow\rangle)$, where $\delta=1.21$ rad. If the spin is measured to be up, the electron orbit aligns parallel to the $\hat{z}$ axis; if the spin is measured to be down, the electron orbit aligns perpendicular to the $\hat{z}$ axis. Thus, the spin is highly correlated with the orientation of the electron orbits. When the precession completes a full cycle, there is no entanglement between the spin and the orbits again. To quantify the variation of the entanglement, the entanglement of formation [23] of Eq. (3), $E(|\Phi\rangle)=-\mathrm{Tr}(\rho_A\log_2\rho_A)=-\mathrm{Tr}(\rho_B\log_2\rho_B)$, is calculated and plotted in Fig. 4, where $\rho_A(\rho_B)$ is the partial trace of $|\Phi\rangle\langle\Phi|$ over one degree of freedom, the spin states or m states. It shows the degree of entanglement changes even when the interaction is constant during the evolution. The mechanism behind this process is quantum interference. If only $P_{3/2}$ is excited, the entangled state and its degree of entanglement is well defined and does not evolve. It is the same if only $P_{1/2}$ is excited. But the coherent excitation of $P_{3/2}$ and $P_{1/2}$ yields a time dependent entanglement due to the nondegenerate energies of the two states. The quantum interference between the two well-defined entanglements in $P_{3/2}$ and $P_{1/2}$ causes the variation of the degree of the entanglement.

In conclusion, we have shown that orthogonal polarized HCPs interact with a Rydberg wave packet in different ways. The redistribution due to a $\hat{z}$-polarized HCP is only allowed if $\Delta\ell=0,1,2\ldots$ and $\Delta m=0$ while the condition for allowed redistribution of an(a) $\hat{x}(\hat{y})$-polarized HCP is $\Delta(\ell+m)=0,2,4\ldots$. Based on these selection rules, the angular precession of an *np* Rydberg wave packet is directly observed by monitoring the population variation of *s* states. The spin degree of freedom has been seen to have a significant influence on the electron wave packet. Its interaction with spatial motion is easily accessed in alkali atoms with large quantum defects using HCPs. Rydberg atoms have been used to demonstrate a unary operations for quantum information processing [24,25]. The coupling of the electron spin to the spatial motion opens the possibility of controlled entanglement between the spin and the spatial wave functions for implementing complex quantum algorithms, where entanglement involving more than one degree of freedom is a requirement [26].

ACKNOWLEDGMENTS

This work has been supported by the National Science Foundation under Grant No. PHY-0456563.

[1] C. O. Reinhold, J. Burgdorfer, M T. Frey, and F. B. Dunning, Phys. Rev. A **54**, R33 (1996).
[2] J. Bromage and C. R. Stroud, Jr., Phys. Rev. Lett. **83**, 4963 (1999).
[3] J. Ahn, D. N. Hutchinson, C. Rangan, and P. H. Bucksbaum, Phys. Rev. Lett. **86**, 1179 (2001).
[4] M. B. Campbell, T. J. Bensky, and R. R. Jones, Phys. Rev. A **59**, R4117 (1999).
[5] H. Wen, S. N. Pisharody, J. M. Murray, and P. H. Bucksbaum, Phys. Rev. A **71**, 013407 (2005).
[6] C. Raman, C. W. S. Conover, C. I. Sukenik, and P. H. Bucksbaum, Phys. Rev. Lett. **76**, 2436 (1996).
[7] R. R. Jones, Phys. Rev. Lett. **76**, 3927 (1996).
[8] M. B. Campbell, T. J. Bensky, and R. R. Jones, Phys. Rev. A **58**, 514 (1998).
[9] W. Zhao, J. C. Lancaster, F. B. Dunning, C. O. Reinhold, and J. Burgdorfer, Phys. Rev. A **69**, 041401(R) (2004).
[10] N. E. Tielking and R. R. Jones, Phys. Rev. A **52**, 1371 (1995).
[11] J. M. Murray, S. N. Pisharody, H. Wen, and P. H. Bucksbaum, Phys. Rev. A **71**, 023408 (2005).
[12] A. tenWolde, L. D. Noordam, A. Lagendijk, and H. B. van Linden van den Heuvell, Phys. Rev. Lett. **61**, 2099 (1988).
[13] J. A. Yeazell and C. R. Stroud, Jr., Phys. Rev. Lett. **60**, 1494 (1988).
[14] J. A. Yeazell, M. Mallalieu, and C. R. Stroud, Jr., Phys. Rev. Lett. **64**, 2007 (1990).
[15] J. A. Yeazell and C. R. Stroud, Jr., Phys. Rev. A **43**, 5153 (1991).

[16] R. Arvieu, P. Rozmej, and M. Turek, Phys. Rev. A **62**, 022514 (2000).
[17] P. Rozmej, M. Turek, R. Arvieu, and I. S. Averbukh, J. Phys. A **35**, 7803 (2002).
[18] J. F. Christian, L. C. Snoek, S. G. Clement, and W. J. van der Zande, Phys. Rev. A **53**, 1894 (1996).
[19] C. Nicole, M. A. Bouchene, S. Zamith, N. Melikechi, and B. Girard, Phys. Rev. A **60**, R1755 (1999).
[20] S. Zamith, M. A. Bouchene, E. Sokell, C. Nicole, V. Blanchet, and B. Girard, Eur. Phys. J. D **12**, 255 (2000).
[21] F. Robicheaux, Phys. Rev. A **56**, R3358 (1997).
[22] A. Wetzels, A. Gürtler, F. Rosca-Prunå, S. Zamith, M. J. J. Vrakking, F. Robicheaux, and W. J. van der Zande, Phys. Rev. A **68**, 041401(R) (2003).
[23] C. H. Bennett, H. J. Bernstein, S. Popescu, and B. Schumacher, Phys. Rev. A **53**, 2046 (1996).
[24] J. Ahn, T. C. Weinacht, and P. H. Bucksbaum, Science **287**, 463 (2000).
[25] J. Ahn, C. Rangan, D. N. Hutchinson, and P. H. Bucksbaum, Phys. Rev. A **66**, 022312 (2002).
[26] P. W. Shor, in *Proceedings of the 35th Annual Symposium on the Foundations of Computer Science*, edited by S. Goldwasser (IEEE Computer Society, Los Alamitos, CA, 1994).